Overpressured fluid injection and fault slip triggering

Yinlin Ji[1], Wei Wu[1] *

[1] Nanyang Technological University, Singapore
* wu.wei@ntu.edu.sg

Background

Harvesting heat trapped in igneous rocks offers us an affordable and sustainable solution to reduce our dependence on fossil fuels. The effectiveness of heat extraction is dependent not only on the permeability of fractured rocks but also on the stability of preexisting and induced faults. In the fluid injection process, when the injection pressure locally exceeds the hydrostatic pressure, fault rupture may occur due to the reduction of effective normal stress and is accompanied by the release of stored strain energy. The Mohr-Coulomb failure criterion describes this process as moving the Mohr circle approaching the failure envelope. However, several lines of evidence show that faults remain stable when the shear stress exceeds the shear strength predicted by the failure criterion (e.g., Scuderi et al., 2017; Rutter and Hackston, 2017). We argue that the abnormal experience is associated with the nonuniform distribution of pore pressure over the fault plane, which is likely affected by in-situ stress condition and fluid injection rate.

Experimental setup and procedure

We investigated the effect of overpressured fluid injection on fault slip triggering in the Bukit Timah granite, a potential geothermal energy source in Singapore. We conducted the triaxial shear-flow experiment (Fig.1a) on a sawcut fault, which was prepared by cutting a 50-mm-diameter and 100-mm-height core sample at 30° to the core axis and polishing the sawcut surfaces using a fine sandpaper with 25.6 μm particle size. We also drilled 2-mm-diameter boreholes parallel to the core axis at the short edges of the sample halves to facilitate distilled water flowing from the core holders to the fault plane. Fig. 1b shows the experimental program in 33 steps, considering injection-induced fault instability under different combinations of effective normal stress and fluid injection rate. First, under 5 MPa effective normal stress, we loaded the sample at an axial displacement rate of 1 μm/s until the fault failed to determine the shear strength (Step 2), and maintained the shear stress equal 80% of the shear strength in the injection process (Step 5). We measured the pore pressure at fault failure and slip rate during fault slip at an injection rate of 0.002 MPa/s. Second, we fixed an effective normal stress of 10 MPa, set the shear stress as 80% of the shear strength measured from the sheared fault (Steps 9, 15 and 21), and recorded the pore pressure and slip rate at three different injection rates, i.e., 0.0004 MPa/s (Step 12), 0.002 MPa/s (Step 18) and 0.01 MPa/s (Step 24). Last, under 20 MPa effective normal stress and subsequently updated shear strength (Step 28), we measured the pore pressure and slip rate again at 0.002 MPa/s injection rate (Step 31). In the meantime, we used acoustic emission sensors to detect strain energy release during the injection-induced fault failure. During the five injection processes, we expect to observe locked fault at relatively high injection rates and violent failure under relatively high effective normal stress.

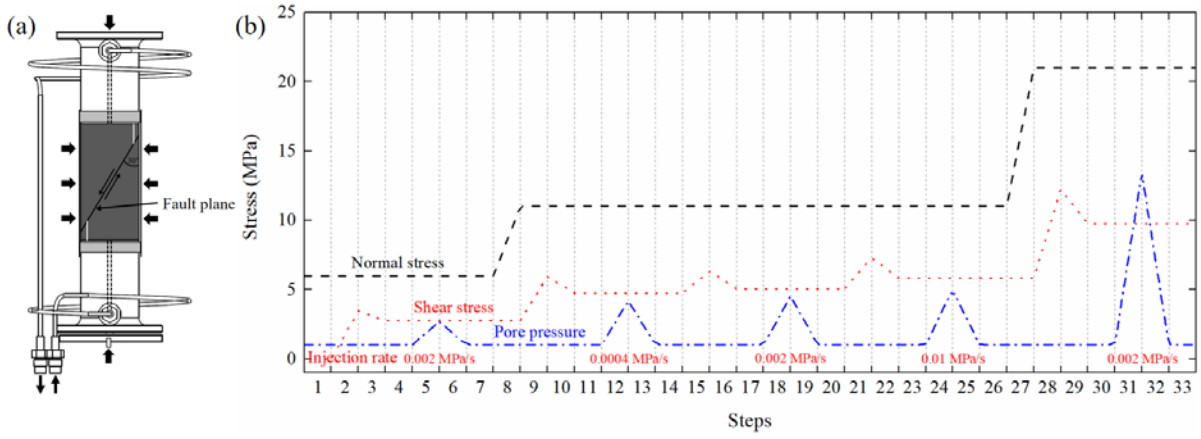

Fig. 1: (a) Triaxial shear-flow experimental setup and (b) injection-induced fault instability under different combinations of effective normal stress and fluid injection rate

Results and discussion

Fig. 2a shows the stress and displacement paths to induce initial fault instability (either stable sliding or stick-slip friction), followed by stabilizing the fault through reducing the shear stress to 80% of the shear strength. In the injection process, maintaining the shear stress and increasing the pore pressure lead to the fault changing from the critical/sub-critical state to the failure state. This procedure is also applied in the subsequent injection processes. The shear strengths obtained from the displacement-driven fault failure under various effective normal stresses are used to plot the failure envelope (Fig. 2b). The friction coefficient of the sawcut fault is 0.63. However, the pore pressure obtained from the injection-induced fault failure exceeds that predicted by the failure criterion. The discrepancy is due to the difference between the pressure measured in the pore system and that predicted on the fault plane. In other words, the nonuniformly distributed pore pressure over the fault plane "apparently" results in the inapplicability of the failure criterion. The ratio between the pore pressure measured at failure and that predicted by the failure criterion, defined as the pore fluid overpressure ratio, increases with higher effective normal stress (Fig. 2c) and greater fluid injection rate (Fig. 2d). Nevertheless, when the injection rate is very high, pore pressure likely accumulates around the injection boreholes, instead of triggering fault slip (see the open point in Fig. 2d). Our results also show that the slip rate raises as the effective normal stress or injection rate increases, indicating that the strain energy release is associated with pore pressure accumulation. This observation is consistent with the acoustic emission signals detected during the injection-induced fault failure, which shows that the relative energy intensity increases from 12,023 mv.μs for 5 MPa effective normal stress to 32,225 mv.μs for 10 MPa to 145,535 mv.μs for 20 MPa. Our future study will consider the nonuniform distribution of pore pressure in natural faults to uncover the mechanism of injection-induced fault rupture and the permeability evolution of overpressured faults (e.g., Wu et al., 2017).

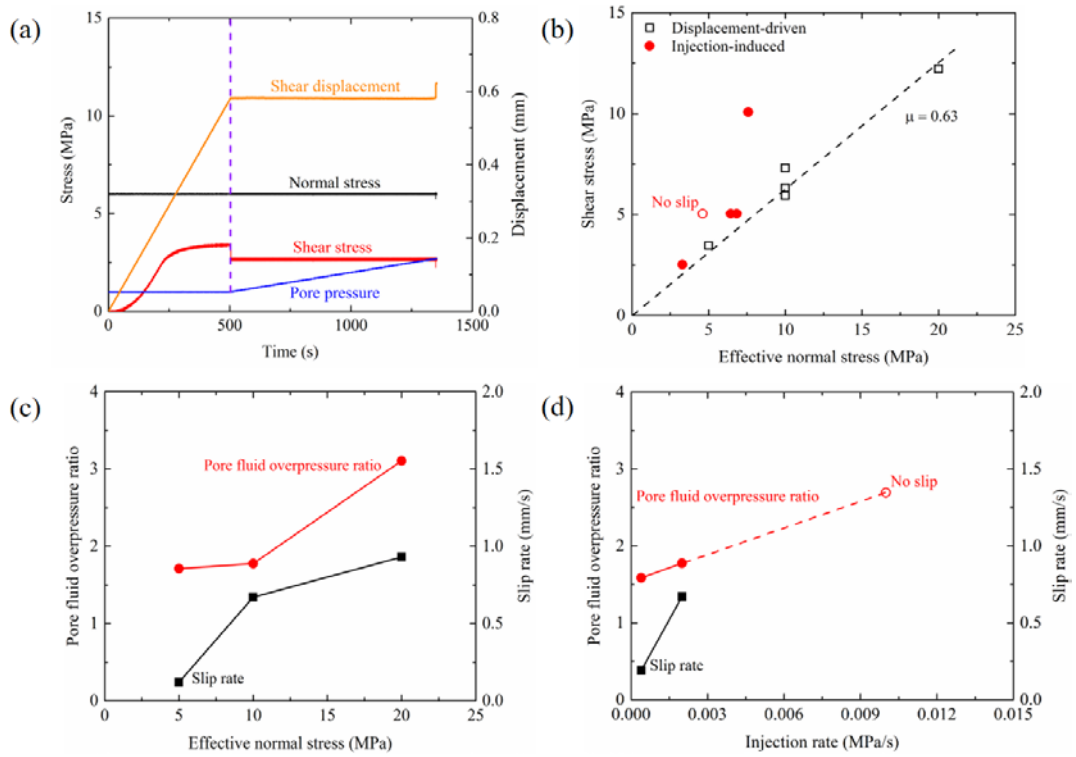

Fig. 2: Experimental results, (a) typical stress and displacement paths before and during the fluid injection process, (b) Mohr-Coulomb failure envelope and effective normal stress measured from the injection-induced fault failure, as well as pore fluid overpressure ratio and slip rate as a function of (c) effective normal stress and (d) injection rate

References

Scuderi MM, Collettini C, Marone C (2017) Frictional stability and earthquake triggering during fluid pressure stimulation of an experimental fault. Earth Planet Sci Lett 477:84-96. doi: 10.1016/j.epsl.2017.08.009

Rutter E, Hackston A (2017) On the effective stress law for rock-on-rock frictional sliding and fault slip triggered by means of fluid injection. Phil Trans R Soc A 375:20160001. doi: 10.1098/rsta.2016.0001

Wu W, Reece JS, Gensterblum Y, Zoback MD (2017) Permeability evolution of slowly slipping faults in shale reservoirs. Geophys Res Lett 44(22):11368-11375. doi: 10.1002/2017GL075506